Phenomenological model for predicting thermoelectromechanical response of 2-2 piezocomposite

Pierre Tize Mha, Pierre Maréchal, Guy Ntamack, Bienvenue Kenmeugne

Phenomenological model for predicting thermoelectromechanical response of 2-2 piezocomposite

Pierre Tize Mha[1], Pierre Maréchal[2], Guy Edgar Ntamack[1], Kenmeugne Bienvenue[3]

Abstract

The homogenization of piezocomposites is a research challenge as the development of analytical models remains a challenge. In this perspective, this work contributes to the development of an analytical model to predict the thermoelectromechanical behavior of the 2-2 piezocomposite where both phases are electrically active. To establish this model the series/parallel method was used and thus the effective homogenized properties of the composite are established. The influence of the volume fraction on the characteristic parameters was studied and found that a numerical simulation of the effective parameters resulting from a {PZT-5A / PVDF-TrFE} composition shows that, volume fraction influences significantly on the properties of the piezocomposite and consequently on its behavior in service. Due to the unavailability of experimental data in the literature, the validation of the model is done with reference to the model applied to the 1-3 piezocomposite. Therefore, to a certain extent, it is found that the results are in agreement. Based on the results of this model and in comparison with those formulated from 1-3 piezocomposite as presented in the paper, the studied 2-2 piezocomposite could be used where 1-3 piezocomposite is sometimes integrated, as the highest performance piezocomposite. However, this remains to be validated experimentally for targeted applications to be be useful for the scientific and even industrial communities.

Keywords: Homogenization, connectivity, electromechanical property, piezoelectric material

1. Introduction

With the advancement of technology in the field of active materials, industries are seeking for the improvement of existing technologies, while reducing the costs and among them the amount of required material and energy resources. For instance, the development of new piezocomposite compositions needs to experiment with various factors on an initially known situation. Smart composite materials are increasingly integrated in the aerospace industry, aeronautics and many other sectors as sensors and/or transducers for noise and vibration control, ageing control and structural health monitoring due to the fact that they are made of piezoelectric materials which

Email addresses: tizemha@yahoo.com (Pierre Tize Mha), pierre.marechal@univ-lehavre.fr (Pierre Maréchal)

[1]GMMA: Groupe de Mécanique, Matériaux et Acoustique, Département de Physique, Faculté des Sciences, Université de Ngaoundéré B.P. 454 Ngaoundéré, Cameroun.

[2]LOMC: Laboratoire Ondes et Milieux Complexes, UMR 6294 CNRS, Université du Havre, France.

[3]The University of Bamenda, P.O.Box 39 Bambili, NW Region, Cameroun.

have the property of converting mechanical energy into electrical energy and vice versa [1]. In aerospace, for example, high-temperature sensors are needed to monitor propulsion systems, to ensure proper operation, and to improve maintenance and safety. These sensors must be able to operate at temperatures in the range from 500 to 1000°C for periods of 100,000 hours [2]. In the automotive field, combustion monitoring is synonymous with efficiency and performance for the improvement of combustion. For this purpose, sensors that can operate at high temperatures are essential for recording combustion, temperature, pressure and engine vibration data. Indeed, combustion sensors must be positioned close to high temperature sources for accurate performance monitoring. In addition, the energy and manufacturing industries are in constant demand for that can operate at high temperatures [3, 4]. For example, the nuclear industry uses and needs sensors for non-destructive testing and for the non-destructive evaluation of various sensitive parts of the plant structure. These sensors allow to monitor the evolution of nuclear fuel rods. On the basis of different materials and piezoelectric compositions [5, 6], this work is aimed at the design and optimization of piezocomposite materials. Due to the ability of piezoelectric materials to couple electrical and mechanical properties, they have been widely used as sensors and transducers in underwater applications [5, 7]. The characterization of a transducer is generally related to two key properties: sensitivity and resolution. The electromechanical coupling coefficient defines the sensitivity of a transducer while the centre frequency and bandwidth define the resolution. In the amount of existing piezoelectric materials, mainly two types of piezoelectric materials were used as transducers in the early days of medical ultrasound imaging: Lead Zirconate Titanate (PZT) and Polyvinylidene Fluoride (PVDF) [8–10]. The acoustic impedance of PZT is high and therefore makes it difficult to send ultrasound energy into human tissue with low acoustic impedance. In addition, the very high Q value of PZT makes the bandwidth narrow and this in turn leads to poor resolution due to noise effects. A piezoelectric polymer such as PVDF has an acoustic impedance that matches that of human tissue, but the electromechanical coupling coefficient is very low, resulting in poor sensitivity. In addition, the low dielectric constant of PVDF also creates the problem of electrical impedance mismatch, which limits the application of PVDF in array transducers [11]. The growth in the market for ferroelectric sensors, actuators and transducers requires continuous improvement and performance of the (piezoelectric) materials in the design of these sensors, actuators and transducers. However, using single-phase piezoelectric materials makes it difficult to improve material properties such as piezoelectric coefficients, acoustic impedance and material density significantly. On the other hand, many composite materials, which incorporate several constituent phases with better properties, offer new and attractive features such as piezoceramics in hydrostatic and medical imaging applications. Since then, piezoelectric materials have been replaced by piezocomposites [12–15]. However, real-world experimentation can be extremely costly and time-consuming for industrial companies, and the results may not be reliable. Obviously, this slows down the company's operating system in the competitive market. It should also be noted that the realization of such an experiment (taking into account the cost factor) is not within the reach of everyone. In view of this situation, it is worth asking whether it is possible to find or even develop a technique that is an alternative that can at least alleviate the effects of the experiment [16, 17]. With this in mind, several techniques have been developed to study piezocomposites [18]. Among the modeling methods, some analytical models have been developed with a view to purely theoretical formulae to obtain the homogenized properties of the piezocomposite [19, 20]. In alternative studies, with a purely numerical approach, the finite element method (FEM) has been developed for complex geometries [21, 22]. As analytical models, Newnham et *al.* [23] developed a model based on notions of series/parallel connectivity for pyroelectric piezocomposites. Banno [24] formulates an analytical model to

perform a study of the coupling of closed and open pore ceramics based on the modified cube model. For more details concerning experimental results referring to the aforementioned works, see [25–28]. Dunn and Taya [29] used Mori-Tanaka (MT) microdifferential theories to establish the electromechanical properties of a piezocomposite in order to study its behavior, as demonstrated recently by Mishra and Das [30]. The Kuo and Huang [31] method based on the notion of anisotropy of 3D inclusions evaluates the properties of these inclusions as the properties related to the phases, the orientation of the angles, the volume fraction and the shape of the inclusions. As for Nan et *al.* [32], they proposed a technique for calculating the effective coefficients of 1-3 (PZT/epoxy) piezocomposite in which the PZT piezoelectric phase are randomly arranged in an epoxy passive polymer matrix using the Green method. Odegard [33] expanded the MT formulation for the prediction of the mechanical properties of chosen piezocomposites. Fakri and Azrar [34] implemented homogenization methods based on incremental self-consistent scheme, improving the classical self-consistent model for piezocomposites, in agreement with predictions based on the MT and self-consistent models. Kar-Gupta and Venkatesh [35] developed a model that takes into account the anisotropy of the fibers to study the behavior of piezocomposite where both phases are active. As highlighted by Chan, Ng and Choy [27, 28] in the case of two-active-phase composites, the resulting piezoelectric coefficients can be enhanced if the phases exhibit opposite polarization. Such a configuration would have a considerable impact on the effective piezoelectric effects, rising the interest of a study under such circumstances. The homogenized coefficients of a composite in general are related to the structure of its constituent cell; in other word, to the properties of the elements of that cell [8, 36–38]. Among the multi-scale methods, as demonstrated by Levassort et *al.* [39, 40], the homogenization method leads to macroscopic characteristics of a heterogeneous material from those of elementary homogeneous phases. Recently, Tize-Mha et *al.* [41] developed an analytical model to deduce the homogenized coefficients and parameters of 1-3 piezocomposite. Of all the above mentioned works, the major part is carried out using 1-3 piezocomposite. However, the 2-2 piezocomposite also plays a very important role in the manufacture of transducers. As works based on this type of piezocomposite, we can mention those of [42–47]. Another form of study consists of reinforcing the performance of the piezocomposites by using a ceramic base which is combined in parallel or in series with the 1-3 or 2-2 piezocomposites which forms the 1-3-2 piezocomposite or the 2-2-2 piezocomposite. We can cite here the works of [7, 12, 31, 48–51]. The design of the 2-2 piezocomposite is in the form of serial or parallel layers with a large interface. Therefore, when this structure is stressed and due to residual stresses, an increase in temperature at the interface can be observed. In addition to the environmental conditions under which the sensors are used, where the temperature may vary, it is therefore important to study the impact of temperature on the properties of these composite materials. In the previous works, the issues related to thermal effects on the effective properties of the piezocomposite are mostly studied in the 1-3 piezocomposite or its derivatives, whereas none of these issues are addressed for the 2-2 piezocomposite. This work therefore consists of taking into account the thermal effects in the determination of the effective coefficients and parameters of the 2-2 piezocomposite. This work is essentially organised in 5 sections. In Section 2, the concept of connectivity is presented. Section 3 presents the formulation of model we propose in this work. Results are presented in Section 4 and then compared and discussed with the 1-3 piezocomposite model in Section 5. while the underwater applications of piezocomposite 2-2 is dedicated to Section 6.

2. Connectivity

To describe how the phases are arranged in a piezocomposite Newnham [23] introduced the notion of connectivity. Suppose a cube isolated from a two-phase piezocomposite. The number of directions by which this cube can be crossed from one side to another following the line of a stop without leaving a considered phase represents the connectivity. As a result, in 3 dimensions, for a two-phase composite material, the connectivities $\{\alpha, \beta\} \in \{0, 1, 2, 3\}$ are giving 16 possible combinations. Since the symmetric cases $\{\alpha, \beta\}$ are resulting from a permutation of phases 1 and 2, the 16 possibilities are reduced to 10 configurations only, as illustrated in the Figure 1 below, with the shaded phase 1 and the clear phase 2.

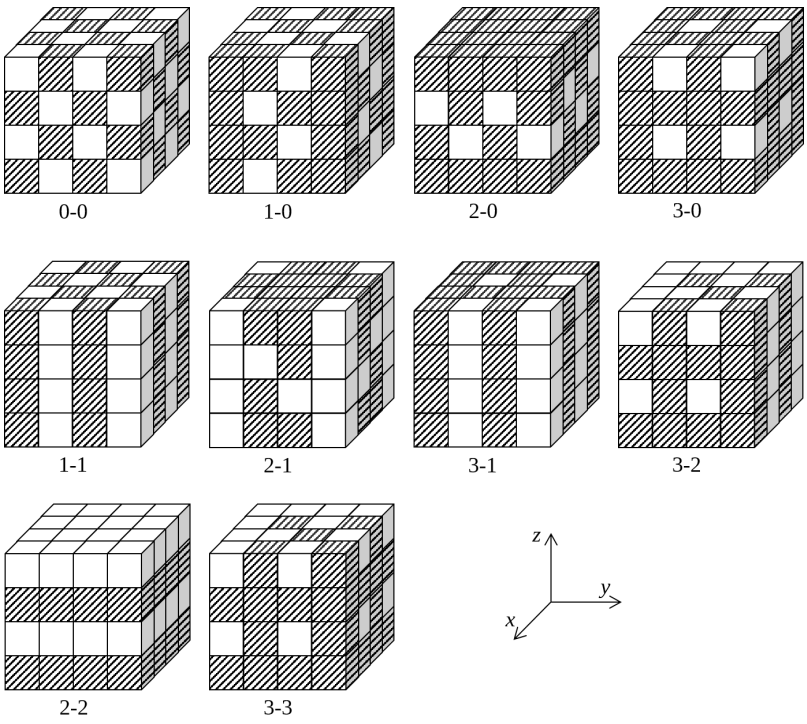

Figure 1: Connectivities of two-phases composite: phase 1 (shaded) and phase 2 (clear), from Newnham [23]

3. Model formulation

Consider the following Figure 2. This figure was extracted from Figure 1 using a simple 90° rotation in the clockwise direction to obtain the current position. Based on this position we see that this configuration can be assimilated to a stack of layers arranged in series along the x-axis and arranged in parallel along the y-axis and z-axis. All subsequent calculations will be based on these two notions of series/parallel. Since the 2-2 composite can be treated as a bulk piezoelectric ceramic, it has piezoelectric linear constitutive equations. In the context of stationary linear response of the thermoelectroelastic piezocomposite, the temperature effect has been considered as [34, 50, 52, 53]:

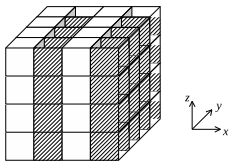

Figure 2: Serial (x axis) and parallel (y and z axes) arrangement of 2-2 piezocomposite layers [23].

$$\begin{cases} T_{ij} = c^E_{ijkl} S_{kl} - e_{ijk} E_k - \beta_{ij} \theta \\ D_i = e_{ikl} S_{kl} - \varepsilon^S_{ij} E_j - P_i \theta \end{cases} \tag{1}$$

To make much easier manipulation of the equations later, reformulation could be done as follows:

$$\begin{cases} T_m = c^E_{mn} S_n - e_{mp} E_p - \beta_m \theta \\ D_q = e_{qn} S_n - \varepsilon^S_{qp} E_p - P_q \theta \end{cases} \tag{2}$$

where the subscript m and n are deduced from ij and kl as follows: $\{ij, kl\} = \{11, 22, 33, 23, 13, 12\}$ and $\{p, q\} = \{1, 2, 3\}$. Transformation of c^E_{ijkl} to c^E_{mn} is done by $m = 9 - (i + j)$ and $n = 9 - (k + l)$ if $i \neq j$ and $k \neq l$, else $m = i = j$ and $n = k = l$. The same procedure can be used to get compact notation of stresses and strains with $\{m, n\} = \{1, 2, 3, 4, 5, 6\}$. In the matrix form, the previous equations can be written as:

$$\begin{bmatrix} T \\ D \end{bmatrix} = \begin{bmatrix} [c^E,] & -[e]^t & -[\beta] \\ [e] & [\varepsilon^S] & [P] \end{bmatrix} \begin{bmatrix} S \\ E \\ \theta \end{bmatrix} \quad \equiv \quad \big[TD\big] = \big[K\beta P\big] \big[SE\theta\big] \tag{3}$$

This writing of the generalized stiffness matrix $\big[K\beta P\big]$ will further be denoted with a superscript $\{m, f\}$ for the matrix and filler phases, respectively. The effective piezocomposite properties will be denoted without any superscript, and the generalized stiffness matrix will be denoted as $\big[K\beta P\big]$. In this study, we consider moreover the z-axis as the polarization axis, then the generalized stiffness matrix $\big[K\beta P\big]$ in detailed form is as follow:

$$\begin{bmatrix} T^x_1 \\ T^x_2 \\ T^x_3 \\ T^x_4 \\ T^x_5 \\ T^x_6 \\ D^x_1 \\ D^x_2 \\ D^x_3 \end{bmatrix} = \begin{bmatrix} c^{Ex}_{11} & c^{Ex}_{12} & c^{Ex}_{13} & 0 & 0 & 0 & 0 & 0 & -e^x_{31} & -\beta^x_1 \\ c^{Ex}_{12} & c^{Ex}_{22} & c^{Ex}_{23} & 0 & 0 & 0 & 0 & 0 & -e^x_{31} & -\beta^x_2 \\ c^{Ex}_{13} & c^{Ex}_{23} & c^{Ex}_{33} & 0 & 0 & 0 & 0 & 0 & -e^x_{33} & -\beta^x_3 \\ 0 & 0 & 0 & c^{Ex}_{44} & 0 & 0 & 0 & -e^x_{24} & 0 & 0 \\ 0 & 0 & 0 & 0 & c^{Ex}_{55} & 0 & -e^x_{15} & 0 & 0 & 0 \\ 0 & 0 & 0 & 0 & 0 & c^{Ex}_{66} & 0 & 0 & 0 & 0 \\ 0 & 0 & 0 & 0 & e^x_{15} & 0 & \varepsilon^{Sx}_{11} & 0 & 0 & P^x_1 \\ 0 & 0 & 0 & e^x_{24} & 0 & 0 & 0 & \varepsilon^{Sx}_{22} & 0 & P^x_2 \\ e^x_{31} & e^x_{32} & e^x_{33} & 0 & 0 & 0 & 0 & 0 & \varepsilon^{Sx}_{33} & P^x_3 \end{bmatrix} \begin{bmatrix} S^x_1 \\ S^x_2 \\ S^x_3 \\ S^x_4 \\ S^x_5 \\ S^x_6 \\ E^x_1 \\ E^x_2 \\ E^x_3 \\ \theta^x \end{bmatrix} \tag{4}$$

where the superscript x stands either for the fiber f or the matrix m or no superscript for the 2-2 piezocomposite. $\big[TD\big] = \big[T, D\big]^t$ is the generalized stress vector including T and D, the stress components and the electrical displacement components respectively; $\big[SE\theta\big] = \big[S, E, \theta\big]^t$

is the generalized strain vector including S, E and θ, the strain components, the electrical field components and the change of temperature respectively; the generalized stiffness matrix $\left[K\beta P\right]$ (4) including $\left\{c^E, e, \varepsilon^S\right\}$ and $\{\beta, P\}$, with c^E the stiffness components at constant electrical field, e the piezoelectric components, ε^S the dielectric components at constant strain, β the thermal coefficients and P the pyroelectric coefficients. The considered piezoelectric materials are in the $4mm$ symmetry class. Thus, their generalized stiffness matrix is with symmetric and having 25 coefficients, and among them 11 independent coefficients. The normal stress in the x-axis of composite, fiber and matrix can be written as:

$$T_1 = c_{11}S_1 + c_{12}S_2 + c_{13}S_3 - e_{31}E_3 - \beta_1\theta \tag{5}$$

$$T_1^f = c_{11}^f S_1^f + c_{12}^f S_2^f + c_{13}^f S_3^f - e_{31}^f E_3^f - \beta_1^f \theta^f \tag{6}$$

$$T_1^m = c_{11}^m S_1^m + c_{12}^m S_2^m + c_{13}^m S_3^m - e_{31}^m E_3^m - \beta_1^m \theta^m \tag{7}$$

3.1. Assumptions

As mentioned in the previous paragraph, the 2-2 piezocomposite can be considered as a sandwich along the x-axis. Indeed, the layers are superimposed on each other along this direction and consequently we have the series hypothesis for this direction. For the other two directions (y-axis and z-axis) the layers are in parallel. Also, the thickness of the second phase is considered proportional to the fiber volume fraction and that the two phases are polarized along the z- axis. All these assumptions have been used in the following calculations.

- **First approximation**:
  The 2-2 piezocomposite is considered as a conventional laminated composite with two layers consisting of fiber as one layer and a matrix as the other one. These layers are in series connectivity in a x-axis; in parallel connectivity in a y-axis and in a z-axis. The homogenized or averaged stress on the fiber layer along the x-direction and the normal stress of the matrix layer that direction are considered to be same. Similarly, the shear stress in (yz) plane are considered to be equal for the fiber and the matrix.

$$\begin{cases} T_1 = T_1^f = T_1^m \\ T_4 = T_4^f = T_4^m \end{cases} \tag{8}$$

- **Second approximation**:
  Along the transverse y-direction and the longitudinal z-direction, the fiber layer and the matrix layer are in parallel connectivity. So, the normal effective stresses for the 2-2 composite those directions can be predicted using the rule of mixtures. The shear stresses (1-3 and 1-2) are obtained by averaging over the contributions of the matrix layer and the fiber layer. With the volume fraction of the fiber and the matrix represented as ν_f and ν_m.

$$\begin{cases} T_2 = \nu_f T_2^f + \nu_m T_2^m \\ T_3 = \nu_f T_3^f + \nu_m T_3^m \\ T_5 = \nu_f T_5^f + \nu_m T_5^m \\ T_6 = \nu_f T_6^f + \nu_m T_6^m \end{cases} \tag{9}$$

- **Third approximation**:
The normal effective strain along the x-axis is calculated based on the individual strain and volume fraction constituents of the 2-2 composite, since they are in series connectivity. The shear strain in the y and z directions is also determined using the weighted sum of fiber layer and matrix layer.

$$\begin{cases} S_1 = \nu_f S_1^f + \nu_m S_1^m \\ S_4 = \nu_f S_4^f + \nu_m S_4^m \end{cases} \tag{10}$$

- **Fourth approximation**:
The homogenized strain on the fiber layer and the normal strain of the matrix layer along the transverse y-axis and the z-axis are considered to be the same by considering the homogeneous displacement condition for the 2-2 piezocomposite. The strains in (xz and xy) planes are considered to be equal for the matrix layer, fiber layer and 2-2 piezocomposite.

$$\begin{cases} S_2 = S_2^f = S_2^m \\ S_3 = S_3^f = S_3^m \\ S_5 = S_5^f = S_5^m \\ S_6 = S_6^f = S_6^m \end{cases} \tag{11}$$

- **Fifth approximation**:
Based on simple theory of the series and parallel connectivity of dielectrics, the effective electrical displacement along the transverse and longitudinal directions can be summed by averaging over the two phases. However, the dielectric displacements are taken to be the same in the x-axis for all. As a consequence, the electric field displacement is determined as the weighted sum of fiber layer and the matrix layer. Along the other directions, the electric fields are considered to be constant.

$$\begin{cases} D_1 = D_1^f = D_1^m \\ D_2 = \nu_f D_2^f + \nu_m D_2^m \\ D_3 = \nu_f D_3^f + \nu_m D_3^m \\ E_1 = \nu_f E_1^f + \nu_m E_1^m \\ E_2 = E_2^f = E_2^m \\ E_3 = E_3^f = E_3^m \end{cases} \tag{12}$$

- **Sixth approximation**:
The change in temperature is assumed to be the same for the fiber layer, the matrix layer and the 2-2 piezocomposite.

$$\theta = \theta^f = \theta^m \tag{13}$$

3.2. Effective coefficients of the 2-2 piezocomposite

From the generalized stiffness matrix $\left[K\beta P\right]$ (4) and taking into account the first, third and sixth assumptions, the formulation starts with replacing the strain components of fiber in equation (6) and 2-2 composite (using (10)), which gives the following relationship:

$$\begin{cases} T_1^f = T_1^m \text{ and } S_1^f = \dfrac{1}{\nu_m}\left(S_1 - \nu_f S_1^f\right) & \Longrightarrow\Downarrow \\ S_1^f = \dfrac{\nu_m c_{11} + \nu_m\left(c_{12}^m - c_{12}^f\right)S_2 + \nu_m\left(c_{13}^m - c_{13}^f\right)S_3 + \nu_m\left(e_{31}^f - e_{31}^m\right)E_3 + \nu_m\left(\beta_1^f - \beta_1^m\right)\theta}{\nu_m c_{11}^f + \nu_f c_{11}^m} \\ S_1^m = \dfrac{\nu_f c_{11} - \nu_f\left(c_{12}^m - c_{12}^f\right)S_2 - \nu_f\left(c_{13}^m - c_{13}^f\right)S_3 - \nu_f\left(e_{31}^f - e_{31}^m\right)E_3 - \nu_f\left(\beta_1^f - \beta_1^m\right)\theta}{\nu_m c_{11}^f + \nu_f c_{11}^m} \end{cases} \tag{14}$$

$$\begin{aligned} T_1^f = \frac{c_{11}^f c_{11}^m}{\nu_m c_{11}^f + \nu_f c_{11}^m} S_1 + \left(c_{12}^f + \frac{\nu_f\left(c_{12}^m - c_{12}^f\right)c_{11}^f}{\nu_m c_{11}^f + \nu_f c_{11}^m}\right) S_2 + \left(c_{13}^f + \frac{\nu_f\left(c_{13}^m - c_{13}^f\right)c_{11}^f}{\nu_m c_{11}^f + \nu_f c_{11}^m}\right) S_3 \\ + \left(-e_{31}^f + \frac{\nu_f\left(e_{31}^f - e_{31}^m\right)c_{11}^f}{\nu_m c_{11}^f + \nu_f c_{11}^m}\right) E_3 + \left(-\beta_1^f + \frac{\nu_f\left(\beta_1^f - \beta_1^m\right)c_{11}^f}{\nu_m c_{11}^f + \nu_f c_{11}^m}\right)\theta \\ = \overline{c}_{11}^E S_1 + \overline{c}_{12}^E S_2 + \overline{c}_{13}^E S_3 - \overline{e}_{31} E_3 - \overline{\beta}_1 \theta \end{aligned} \tag{15}$$

Five effective properties can be deduced from the above equation and the same procedure with other assumptions is used to get the rest of effective properties. Thus all effective properties of the 2-2 piezocomposite are given bellow:

For the elastic coefficients, we have:

$$\begin{cases} \overline{c}_{11}^E = \dfrac{c_{11}^f c_{11}^m}{c_{11}^{mf}}\ ,\ c_{11}^{mf} = \nu_f c_{11}^m + \nu_m c_{11}^f \\ \overline{c}_{12}^E = c_{12}^f + \dfrac{\nu_m c_{11}^f}{c_{11}^{mf}}\left(c_{12}^m - c_{12}^f\right) \\ \overline{c}_{13}^E = c_{13}^f + \dfrac{\nu_m c_{11}^f}{c_{11}^{mf}}\left(c_{13}^m - c_{13}^f\right) \\ \overline{c}_{22}^E = \left(\nu_f c_{22}^f + \nu_m c_{22}^m\right) - \dfrac{\nu_m \nu_f}{c_{11}^{mf}}\left(c_{12}^m - c_{12}^f\right)^2 \\ \overline{c}_{23}^E = \left(\nu_f c_{23}^f + \nu_m c_{23}^m\right) - \dfrac{\nu_m \nu_f}{c_{11}^{mf}}\left(c_{13}^m - c_{13}^f\right)\left(c_{12}^m - c_{12}^f\right) \\ \overline{c}_{33}^E = \left(\nu_f c_{33}^f + \nu_m c_{33}^m\right) - \dfrac{\nu_m \nu_f}{c_{11}^{mf}}\left(c_{13}^m - c_{13}^f\right)^2 \\ \overline{c}_{44}^E = \dfrac{c_{44}^f c_{44}^m}{c_{44}^{mf}}\ ,\ c_{44}^{mf} = \nu_f c_{44}^m + \nu_m c_{44}^f \\ \overline{c}_{55}^E = \left(\nu_f c_{55}^f + \nu_m c_{55}^m\right) - \dfrac{\nu_m \nu_f}{\varepsilon_{11}^{mf}}\left(e_{15}^m - e_{15}^f\right)^2 \\ \overline{c}_{66}^E = \left(\nu_f c_{66}^f + \nu_m c_{66}^m\right)\ ,\ \varepsilon_{11}^{mf} = \nu_f \varepsilon_{11}^m + \nu_m \varepsilon_{11}^f \end{cases} \tag{16}$$

The piezoelectric coefficients are:

$$\begin{cases} \overline{e}_{31} = e_{31}^f + \dfrac{\nu_m c_{11}^f}{c_{11}^{mf}} \left(e_{31}^m - e_{31}^f \right) \\ \overline{e}_{32} = \left(\nu_f e_{32}^f + \nu_m e_{32}^m \right) - \dfrac{\nu_f \nu_m}{c_{11}^{mf}} \left(e_{31}^m - e_{31}^f \right) \left(c_{12}^m - c_{12}^f \right) \\ \overline{e}_{33} = \left(\nu_f e_{33}^f + \nu_m e_{33}^m \right) - \dfrac{\nu_f \nu_m}{c_{11}^{mf}} \left(e_{31}^m - e_{31}^f \right) \left(c_{13}^m - c_{13}^f \right) \\ \overline{e}_{24} = e_{24}^f + \dfrac{\nu_m c_{44}^f}{c_{44}^{mf}} \left(e_{24}^m - e_{24}^f \right) \\ \overline{e}_{15} = e_{15}^f + \dfrac{\nu_m \varepsilon_{11}^f}{\varepsilon_{11}^{mf}} \left(e_{15}^m - e_{15}^f \right) \end{cases} \tag{17}$$

The dielectric coefficients are:

$$\begin{cases} \overline{\varepsilon}_{11}^S = \dfrac{\varepsilon_{11}^f \varepsilon_{11}^m}{\varepsilon_{11}^{mf}} \\ \overline{\varepsilon}_{22}^S = \left(\nu_f \varepsilon_{22}^f + \nu_m \varepsilon_{22}^m \right) + \dfrac{\nu_f \nu_m}{c_{44}^{mf}} \left(e_{24}^m - e_{24}^f \right)^2 \\ \overline{\varepsilon}_{33}^S = \left(\nu_f \varepsilon_{33}^f + \nu_m \varepsilon_{33}^m \right) + \dfrac{\nu_f \nu_m}{c_{11}^{mf}} \left(e_{31}^m - e_{31}^f \right)^2 \end{cases} \tag{18}$$

The thermal coefficients are:

$$\begin{cases} \overline{\beta}_1 = \beta_1^f + \dfrac{\nu_m c_{11}^f}{c_{11}^{mf}} \left(\beta_1^m - \beta_1^f \right) \\ \overline{\beta}_2 = \left(\nu_f \beta_2^f + \nu_m \beta_2^m \right) - \dfrac{\nu_f \nu_m}{c_{11}^{mf}} \left(\beta_1^m - \beta_1^f \right) \left(c_{12}^m - c_{12}^f \right) \\ \overline{\beta}_3 = \left(\nu_f \beta_3^f + \nu_m \beta_3^m \right) - \dfrac{\nu_f \nu_m}{c_{11}^{mf}} \left(\beta_1^m - \beta_1^f \right) \left(c_{13}^m - c_{13}^f \right) \end{cases} \tag{19}$$

And finally, the pyroelectric coefficients are given by:

$$\begin{cases} \overline{P}_1 = P_1^f + \dfrac{\nu_m \varepsilon_{11}^f}{\varepsilon_{11}^{mf}} \left(P_1^m - P_1^f \right) \\ \overline{P}_2 = \nu_f P_2^f + \nu_m P_2^m \\ \overline{P}_3 = \left(\nu_f P_3^f + \nu_m P_3^m \right) + \dfrac{\nu_f \nu_m}{c_{11}^{mf}} \left(e_{31}^m - e_{31}^f \right) \left(\beta_1^m - \beta_1^f \right) \end{cases} \tag{20}$$

To evaluate the performance of a piezocomposite, usually its effective parameters ($\overline{Z}_L, \overline{c}_L$ and $\overline{k}_t$) are determined by the following equations:

$$\begin{cases} \overline{c}_{33}^D = \overline{c}_{33}^E + \frac{(\overline{e}_{33})^2}{\overline{\varepsilon}_{33}^S} \\ \overline{h}_{33} = \frac{\overline{e}_{33}}{\overline{\varepsilon}_{33}^S} \end{cases} \tag{21}$$

From the effective mass density $\overline{\rho} = \nu_f \rho^f + \nu_m \rho^m$ we can express the various effective parameters as bellow:

$$\begin{cases} \overline{Z}_L = \sqrt{\overline{c}_{33}^D \overline{\rho}} \\ \overline{c}_L = \sqrt{\frac{\overline{c}_{33}^D}{\overline{\rho}}} \\ \overline{k}_t = \frac{\overline{e}_{33}}{\sqrt{\overline{c}_{33}^D \overline{\varepsilon}_{33}^S}} \end{cases} \tag{22}$$

4. Results

After the development of the model in the previous section, now time to analysis and interpretation of the numerical results of the developed model. It should be recalled that the establishment of the proposed model in this study is based on the simultaneous consideration of thermal, electrical, piezoelectric and pyroelectric effects. Thus, it is possible that the results are presented separately in the rest of the document. In this study, the piezoelectric materials PVDF-TrFE copolymer (polyvinylidene fluoride-trifluoroethylene) and PZT-5A are used as matrix and fiber, respectively. The properties of the materials used in the study are presented in Table 1. The stress–temperature moduli β_i in equation (3), are given in the two last lines of Table 1 as a result of equation (23), *i.e.* the sum of the products of c_{ij}^E the stiffness components at constant electrical field by α_i the linear thermal expansion coefficients.

$$\beta_i = \sum_{j=1}^{j=3} c_{ij}^E \alpha_i \tag{23}$$

The main purpose of the study is to assess the influence of the volume fraction and the active properties of the matrix on the effective thermoelectromechanical properties of 2-2 piezocomposite. As no experimental results are available in the literature, the validation of the proposed model is based on analytical models available in the literature such as the Cha model [54].

Table 1: Electromechanical properties of piezoelectric materials [44]

Parameters	PZT-5A	PVDF/TrFE
c_{11}^E (GPa)	126	8.5
c_{12}^E (GPa)	79.5	3.6
c_{13}^E (GPa)	84.1	3.6
c_{33}^E (GPa)	109	9.9
c_{44}^E (GPa)	23	1.9
c_{66}^E (GPa)	23.5	2.45
e_{31} (C/m^2)	-6.5	0.008
e_{33} (C/m^2)	24.8	-0.29
$\varepsilon_{11}^S/\varepsilon_0, \varepsilon_{22}^S/\varepsilon_0$	1700	7.5
$\varepsilon_{33}^S/\varepsilon_0$	1813	9.0
$\alpha_1, \alpha_2, \alpha_3$ (K^{-1})	1.2×10^{-6}	0.18×10^{-6}
P_1, P_2, P_3 (C/m^2/K)	2.5×10^{-5}	2.0×10^{-5}
ρ (kg/m^3)	7898	1880
β_1, β_2 (Pa/K)	34.75×10^4	2826
β_3 (Pa/K)	33.26×10^4	3078

In this work, the thermoelectromechanical coefficients of the 2-2 piezocomposite are established using the unsimplified form of the stiffness matrix $\left[K\beta P\right]$ (4). Only during the numerical modeling some coefficients of the matrix (respectively of the fiber) were assimilated identical because of the symmetry of the problem. It should be noted that the 2-2 piezocomposite has its two phases both active. Obtaining these coefficients allowed to establish the effective parameters of the piezocomposite, thus allowing to evaluate the performance or at least the serviceability of the piezocomposite.

Figure 3 shows the homogenized coefficients and the effective parameters of the 2-2 piezocomposite using the model established in Section 3, all the curves obtained from which are compared to those obtained by two models in the literature (Cha [54] and Reuss [55] models).

As illustrated by Figure 3a, the elastic coefficient $\overline{c}_{33}^{E}$ given by the Reuss model underestimates the values obtained for the Cha and proposed models. For low values of the volume fraction, between 0% and 50% for the Reuss model, a slow evolution of the elastic coefficient $\overline{c}_{33}^{E}$ is observed. Between 0% and 80% for the Cha and proposed model, the elastic coefficient $\overline{c}_{33}^{E}$ increases linearly. It should be noted that the Reuss curve occupies a lower bound to what is predicted by the laws of composite materials in general. It can also be noted that the Cha model and proposed model are similar in this case. For the volume fraction values between 75% and 100%, an exponential evolution of this coefficient is observed. For the relative dielectric coefficient $\overline{\varepsilon}_{33}^{S}/\varepsilon_0$ (Figure 3b), the curves obtained with the Reuss, Cha and proposed models evolve linearly with the volume fraction. The effective piezoelectric coefficient $\overline{e}_{33}$ (Figure 3c) has linear evolution for the Cha and proposed models with a volume fraction between 0% and 90% whereas a parabolic evolution is observed for a volume fraction between 90% and 100%. The Reuss model a linear evolution, which is not so far from the two models for this coefficient. The effective piezoelectric coefficient $\overline{e}_{31}$ (Figure 3d) exhibits negative values. The Reuss model presents a linear evolution, decreasing from the value of the PVDF/TrFE downto that of the PZT-5A for a volume fraction of 0% and 100%, respectively. The Voigt model is shown here, because no litteral expression is proposed by the Cha's model. The proposed model has a non linear evolution, which contributes to the deviation from linearity of the $\overline{e}_{33}$ coefficient. Concerning the elastic coefficients at constant displacement $\overline{c}_{33}^{D}$ (Figure 3e), it appears to be the same whatever the model. The differences observed with $\overline{c}_{33}^{E}$ (Figure 3a are related to the thickness coupling coefficient $\overline{k}_t$ (Figure 3f since $\overline{c}_{33}^{E} = \overline{c}_{33}^{D}.(1 - \overline{k}_t^2)$. As a consequence, the thickness coupling coefficient $\overline{k}_t$ (Figure 3f) exhibits strong variations as defined by equation (22). Following the Cha and proposed models, the maximum thickness coupling coefficient $\overline{k}_t$ is reached at $\overline{k}_t$ = 64% for a volume fraction ν_f around 60%. A quasi constant value is obtained for the Cha's model and the proposed model for the volume fraction from ν_f = 40% to 80%. For low values of the volume fraction from ν_f = 0% to 20%, the thickness coupling coefficient $\overline{k}_t$ varies quickly for Cha's model and the proposed model, whereas the Reuss's model follow the same tendency with a slight overestimation for values between 20% and 90%. For very low values of the volume fraction from ν_f < 2%, the thickness coupling coefficient $\overline{k}_t$ is observed to have negative values, what is due to the definition of this parameter (equation (22)) and the negative value of the parameter $\overline{e}_{33}$ for the PVDF/TrFE.

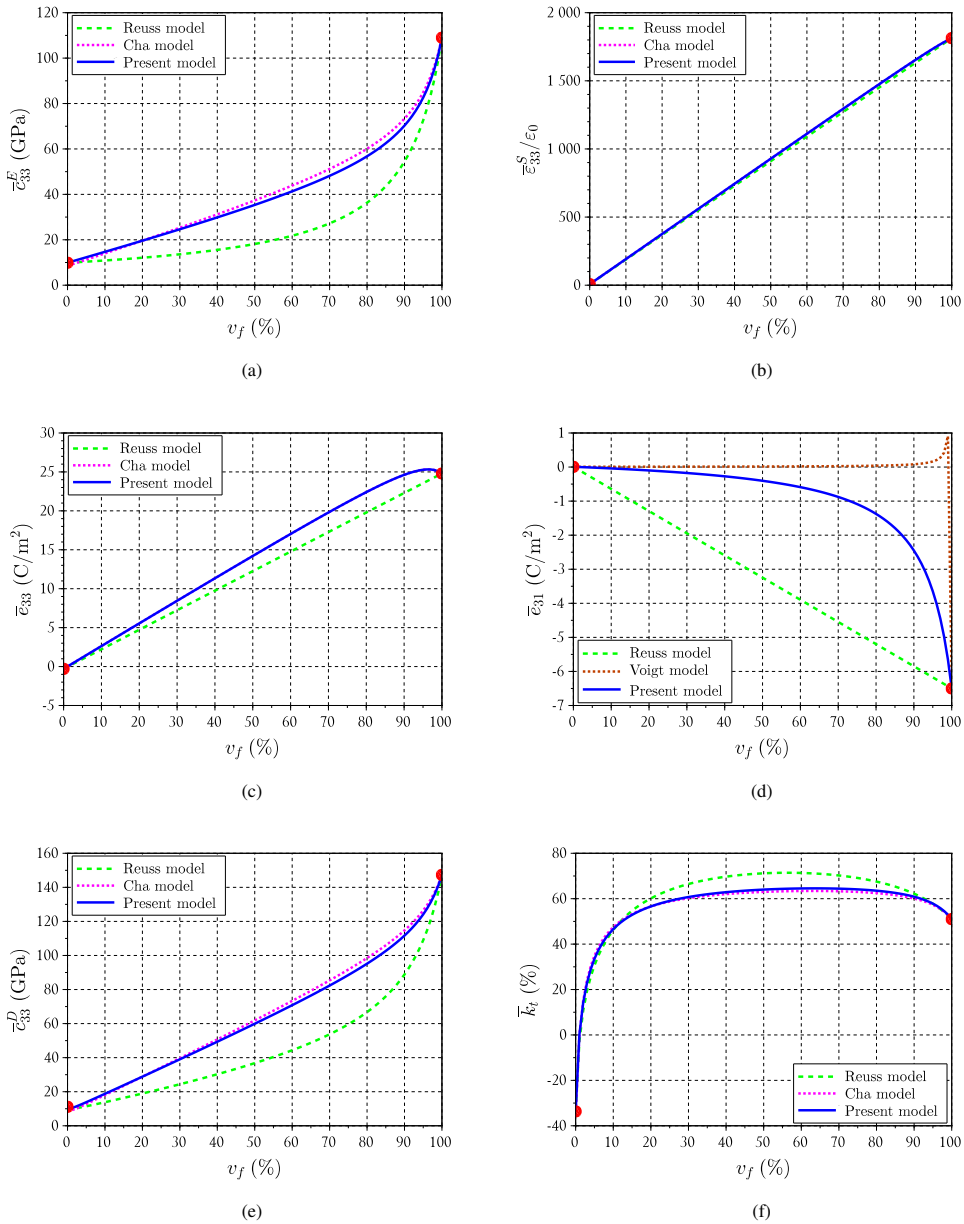

Figure 3: Homogenized coefficients and actual parameters of 2–2 piezocomposite made of a {PZT-5A / PVDF-TrFE} as a function of the volume fraction ν_f: (a) elastic coefficient at constant electric field $\overline{c}^E_{33}$; (b) relative dielectric coefficient at constant strain $\overline{\varepsilon}^S_{33,r}/\varepsilon_0$; (c) and (d) piezoelectric coefficients $\overline{e}_{33}$ and $\overline{e}_{31}$; (e) elastic coefficient at constant electric displacement $\overline{c}^D_{33}$; (f) thickness coupling coefficient $\overline{k}_t$.

For low values of the volume fraction from ν_f = 0% to 30%, the effective longitudinal wave velocity $\overline{c}_L$ (Figure 4a) shows a quick evolution for the Cha and proposed models. For values between 30% and 80%, a quasi linear evolution is observed for these two models. The Reuss model shows a lower increase than for the two other models and clearly underestimates this parameter. As illustrated in Figure 4b, the acoustic impedance $\overline{Z}_L$ shows a nearly linear behavior as a function of the volume fraction ν_f up to 85% for the Cha and proposed models, whereas the Reuss model is giving a slightly lower value. This acoustic impedance is a key parameter in the sense of the acoustic energy transfer between two materials *i.e.* the piezocomposite and the transmission medium. As the acoustic impedance value of the ceramic is generally around 35 MRa, the integration of the ceramic in a polymer matrix allows to modulate and customize this parameter for the targeted application. In order to ensure the proper application of piezoelectric materials, it is important to study the performance of the devices in which they are most often used. On the one hand, the efficiency of the conversion between electrical and acoustic energy (or vice versa) in a piezoelectric material is quantified by the electromechanical coupling coefficient $\overline{k}_t$ (Figure 3f). On the other hand, the energy transfer from the piezocomposite medium is resulting from the acoustical environment, *i.e.* back and front media, and the effective acoustical impedance $\overline{Z}_L$ (Figure 4b) of the piezocomposite thus determines the operating bandwidth [46, 47]. The combination of the adjustable thickness coupling coefficient $\overline{k}_t$ (Figure 3f) and acoustic impedance $\overline{Z}_L$ lead to a possible choice of trade-off for the targeted application. For instance, a medical imaging application will drive the choice of composition to low volume fractions ν_f around 20%, while a NDT contact transducer will drive the choice to higher volume fractions ν_f around 70%. For an optimization of the piezocomposite composition, a specific approach integrating both the acoustical and electrical environments and their frequency dependence can be adopted [41]. Therefore, thanks to the two-way insertion loss, the energy conversion efficiency can be evaluated to bring quantitative estimators for the targeted application.

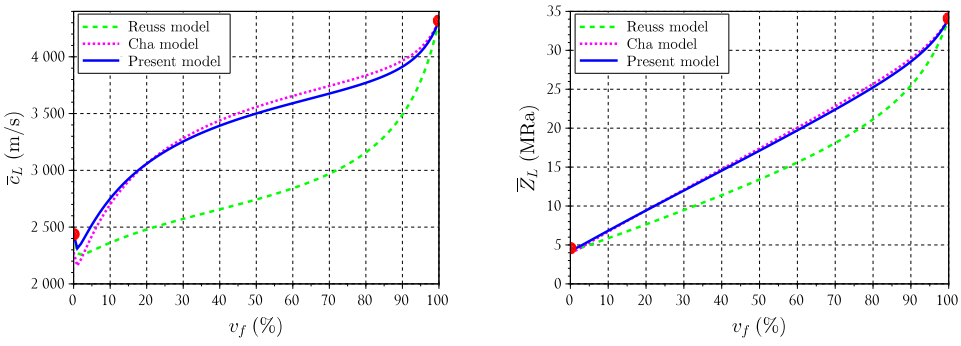

Figure 4: Homogenized longitudinal acoustic parameters of 2–2 piezocomposite made of a {PZT-5A / PVDF-TrFE} as a function of the volume fraction ν_f: (a) longitudinal wave velocity $\overline{c}_L$ and (b) longitudinal acoustical impedance $\overline{Z}_L$.

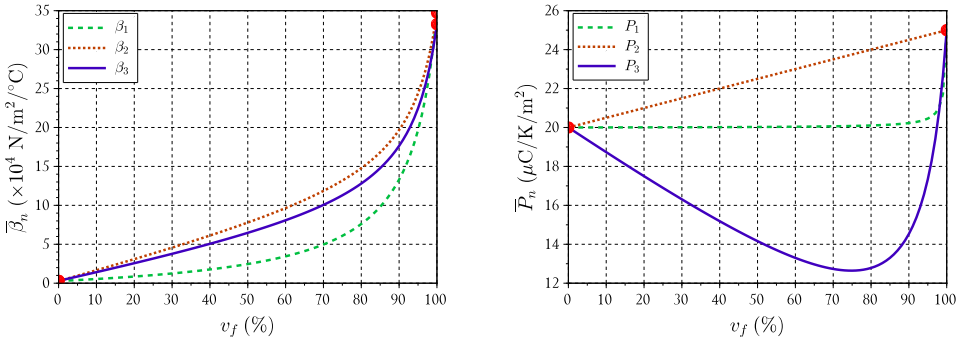

(a) (b)

Figure 5: Homogenized temperature sensitive parameters of 2–2 piezocomposite made of a {PZT-5A / PVDF-TrFE} as a function of the volume fraction ν_f: (a) thermal coefficients β and (b) pyroelectric coefficient P.

The differences observed from these models can be analyzed simply as a matter of formulation of each model. Already the Reuss and Cha models are formulated on the basis of a piezocomposite where one phase (the matrix phase) is passive whereas the proposed model is formulated on the basis of a piezocomposite where both phases are active. Also the calculation assumptions are not identical. The Reuss model is essentially built on the components of the main diagonal of the K-matrix and therefore is dedicated only to tensile and compression effects and nothing else, which is not the case for the other two models. Hence, the behavior of the Reuss model differs from the other models. Few works exist on this type of piezocomposite where the thermal effects are taken and both phases are active for the homogenization of the piezocomposite. Active structures incorporating intelligent materials are often not free from environments influenced by thermal effects and therefore directly affect these materials. Face of these effects, the materials must have good heat resistance and rigidity. However, the variation of temperature in a composite induces ageing. When the structure is subjected to thermal loads beyond a permissible limit, this induces additional thermal stresses in the structure and thus induces deformation. These induced thermal stresses can be reduced by the appropriate choice of combination of thermal parameters $\{\beta, P\}$ of piezoelectric materials. Temperature variation due to internal (high power emission) or external (hot environment) sources, such as temperature in the vicinity of the Curie temperature reached repeatedly, can cause the depolarization of the piezoelectric material. Figure 5a shows the evolution of the thermal and pyroelectric coefficients of piezocomposite 2-2 as a function of the volume fraction ν_f. An important value of the pyroelectric coefficient implies a high sensitivity of a piezocomposite to the thermal change. As illustrated by Figure 5b, the pyroelectric coefficient P_3 in the longitudinal direction 3 decreases linearly down to nearly 12 μC/K/m^2 and then increases up to that of the pyroelectric coefficient P_2 in direction 2. On the other hand, for the pyroelectric coefficient P_1 in direction 1, the evolution is linear. Compared with the results generally obtained on 1-3 piezocomposite, the changes following directions 1 and 2 are identical for both coefficients. This is not the case for the model proposed in this study for the 2-2 piezocomposite, but overall the results are similar to those of 1-3 piezocomposite.

5. Comparison of proposed model and 1-3 piezocomposite model

This section presents a comparison between the results of models developed using the 2-2 piezocomposite and a model developed using the 1-3 piezocomposite. Reuss, Cha and the proposed models are used to obtain the effective properties for the 2-2 piezocomposite while Sakthivel model is used for the 1-3 piezocomposite. Only $\overline{c}_{33}^{E}$, $\overline{\varepsilon}_{33}$, $\overline{k}_t$ and $\overline{Z}_L$ are shown for comparison. The Reuss [55], Cha [54] and Sakthivel [50] models are given as follows:

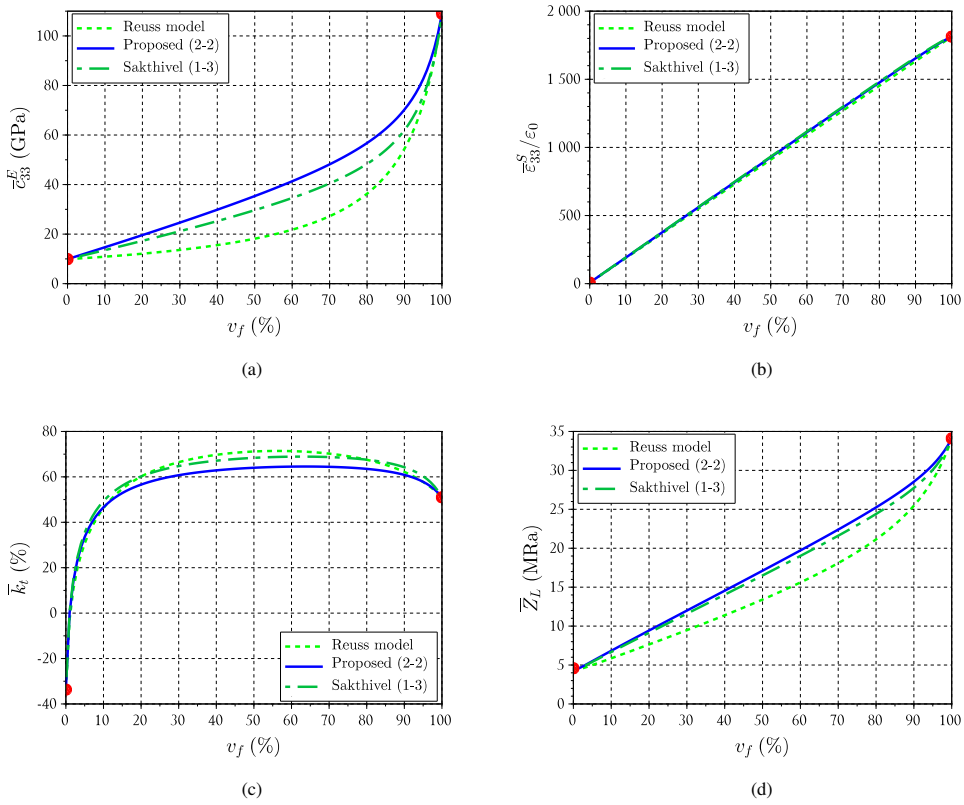

Figure 6: Comparison of homogenized coefficients and actual parameters of 2–2 piezocomposite and 1-3 piezocomposite made of a {PZT-5A / PVDF-TrFE} as a function of the volume fraction ν_f : (a) elastic coefficient at constant electric field $\overline{c}_{33}^{E}$; (b) relative dielectric coefficient at constant strain $\overline{\varepsilon}_{33}^{S}/\varepsilon_0$; (c) thickness coupling coefficient $\overline{k}_t$; (d) acoustic impedance $\overline{Z}_L$.

- Reuss model

$$\begin{cases} \overline{c}_{33}^{E} = \frac{c_{33}^{f} c_{33}^{m}}{\nu_f c_{33}^{m} + \nu_m c_{33}^{f}} \\ \overline{e}_{33} = \nu_f e_{33}^{f} + \nu_m e_{33}^{m} \\ \overline{\varepsilon}_{33}^{S} = \nu_f \varepsilon_{33}^{f} + \nu_m \varepsilon_{33}^{m} \end{cases} \tag{24}$$

- Cha model

$$\begin{cases} \overline{c}_{33}^{E} = \nu_f c_{33}^{f} + \nu_m c_{11}^{m} - \nu_f \nu_m \frac{\left(c_{13}^{f} - c_{12}^{m}\right)^2}{c_{11}^{mf}} \\ \overline{e}_{33} = \nu_f e_{33}^{f} - \nu_f \nu_m \frac{e_{31}^{f}\left(c_{13}^{f} - c_{12}^{m}\right)}{c_{11}^{mf}} \\ \overline{\varepsilon}_{33}^{S} = \nu_f \varepsilon_{33}^{S} + \nu_m \varepsilon_{11}^{m} + \nu_f \nu_m \frac{\left(e_{31}^{f}\right)^2}{c_{11}^{mf}} \end{cases} \tag{25}$$

- Sakthivel model

$$\begin{cases} \overline{c}_{33}^{E} = \nu_f \left(c_{33}^{f} + c_{31}^{f} A_3 + c_{32}^{f} B_3 - c_{31}^{m} A_3 - C_{32}^{m} B_3 \right) + \nu_m c_{33}^{m} \\ \overline{e}_{33} = \nu_f \left(e_{33}^{f} + c_{31}^{m} A_4 + c_{32}^{m} B_4 - c_{31}^{f} A_4 - c_{32}^{f} B_4 \right) - \nu_m e_{33}^{m} \\ \overline{\varepsilon}_{33}^{S} = \nu_f \left(\varepsilon_{33}^{f} + e_{31}^{f} A_4 + e_{32}^{f} B_4 - e_{31}^{m} A_4 - e_{32}^{m} B_4 \right) + \nu_m \varepsilon_{33}^{m} \end{cases} \tag{26}$$

  where the required constants A_i and B_i can be found in [50]

This Figure 6 for the 1-3 piezocomposite is compared with Figure 3 with the model developed for the 2-2 piezocomposite. From these curves it is found that the two models correlate well with discrepancies between the two models only for volume fractions greater than 50%.

6. Underwater applications

Piezocomposites with two active phases can be used in the manufacture of new ultrasonic transducers. In these transducers, ceramic is used for signal emission and the copolymer provides a better electrical and acoustic matching to the input and output signals [37]. The fact that the two phases are active makes it possible to place these phases in opposite directions and therefore improve the piezoelectric coupling effect that is used in the design of the robust transducers. In the literature, there are few works where the two phases are piezoelectrically active. Therefore, the study of the effective properties of these piezocomposites is of paramount importance. Such piezocomposites are typically used either for ultrasonic underwater transducers or hydrophone applications [37, 44, 50]. Taking into account the hydrostatic environment, their performance can estimated on the basis of specific hydrostatic coefficients and thermal environment. As evoked in the introduction, underwater applications not only refer to the SONAR marine transducers, but also encloses industrial applications such as nuclear power plant monitoring and associated high temperature environment. In the context of underwater applications, 2-2 piezocomposites are subjected to temperature variations: lower temperature due to the underwater depth in listening mode or not in service, and higher temperature environment and in the case of power dissipation while operating in sonar application. Thus, the classical generalized stiffness matrix $\left[K\beta P\right]$, where $\left[TD\right] = \left[K\beta P\right]\left[SE\theta\right]$, is impacted by the temperature θ. In this work, the effect of the temperature parameter is integrated in the matrix formulation (4), involving the thermal β and pyroelectric P coefficients. Therefore, in the end, they are inducing drift due to the temperature on the effective thickness parameters, *i.e.* the homogenized thickness parameters $\{\overline{c}_{33}^{D}, \overline{e}_{33}, \overline{\varepsilon}_{33}^{S}\}$ and associated acoustical properties are sensitive to the temperature θ.

Among those figures of merit (FOM), one can cite the hydrostatic charge $\overline{d}_h$, the hydrostatic voltage coefficient $\overline{g}_h$, the hydrophone trade-off $\overline{d}_h\overline{g}_h$ or the hydrostatic electromechanical coupling factor $\overline{k}_h$. These are defined as follows:

$$\begin{cases} \overline{d}_h = \overline{d}_{31} + \overline{d}_{32} + \overline{d}_{33} \\ \overline{s}_h = \overline{s}_{11} + \overline{s}_{22} + \overline{s}_{33} + 2(\overline{s}_{12} + \overline{s}_{13} + \overline{s}_{23}) \\ \overline{g}_h = \frac{\overline{d}_h}{\overline{\varepsilon}^T_{33}} \\ \overline{k}_h = \frac{\overline{d}_h}{\sqrt{\overline{s}_h \overline{\varepsilon}^T_{33}}} \end{cases} \tag{27}$$

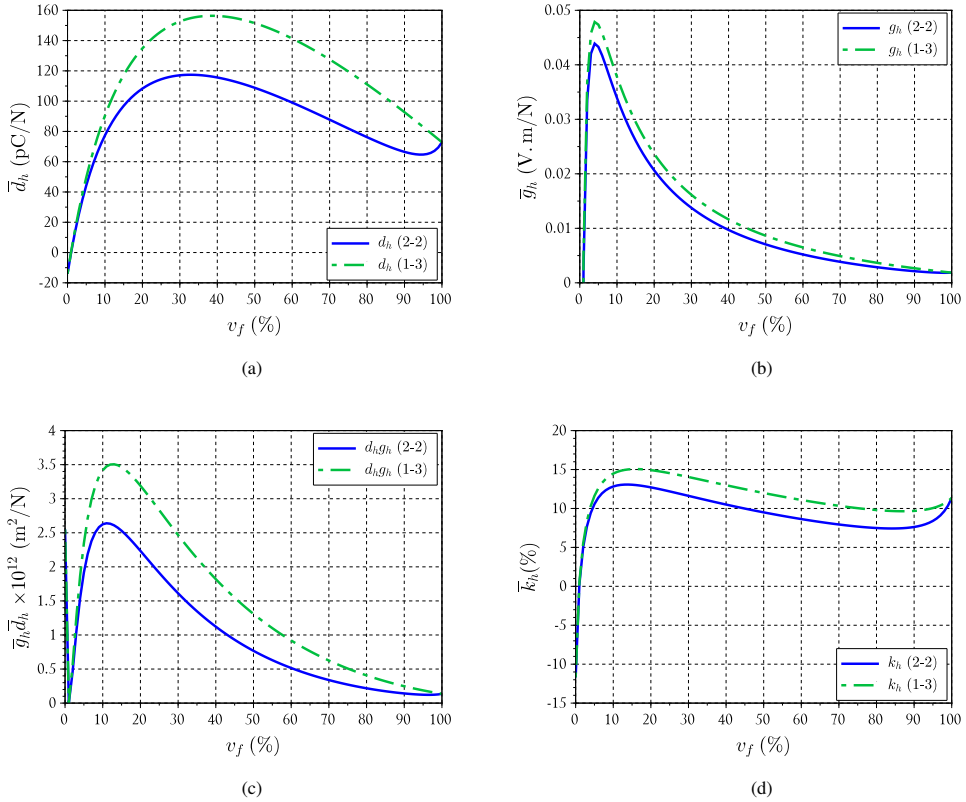

Figure 7: Homogenized electroacoustic properties of the {PZT-5A / PVDF-TrFE} 2-2 piezocomposite as a function of the PZT-5A volume fraction ν_f: (a) effective hydrostatic charge constant $\overline{d}_h$, (b) hydrostatic voltage $\overline{g}_h$, (c) hydrostatic trade-off $\overline{g}_h\overline{d}_h$ (d) hydrostatic electromechanical coupling factor constant $\overline{k}_h$

In the studied {PZT-5A / PVDF-TrFE} 2-2 piezocomposite composition (Table 1), the homogenized piezoelectric properties are analyzed through indirect coefficients deduced from the homogenized generalized stiffness matrix $\left\{\overline{c}^E_{ij}, \overline{e}_{ij}, \overline{\varepsilon}^S_{ij}\right\}$. Based on this result, the generalized compliance matrix $\left\{\overline{s}^E_{ij}, \overline{d}_{ij}, \overline{\varepsilon}^T_{ij}\right\}$ is determined by matrix inversion and classical relations of piezoelectricity. As an application, the hydrostatic FOM (equation (27)) are illustrated (Figure 7). Thus, the hydrostatic charge $\overline{d}_h$ (Figure 7a) shows a very fast evolution for volume fraction values lower than 10% and presents a maximum for a volume fraction around 30% and 50% for the 2-2 and 1-3 connectivities, respectively. The values of hydrostatic voltage $\overline{g}_h$ (Figure 7b) and hydrophone trade-off $\overline{d}_h\overline{g}_h$ (Figure 7c) evolve in a similar way with a maximum value observed

for volume fractions ν_f around 5% and 10%, respectively. A similar observation is made for the hydrostatic coupling factor $\overline{k}_h$ (Figure 7d). Those results are similar to those obtained by Sakthivel [44] for the 1-3 piezocomposite. For more details on each term of this equation, have a look to the appendices.

7. Conclusion

In this work, the consideration of thermal and pyroelectric effects allowed the development of an analytical model for the 2-2 piezocomposite. This leads to deduce the actual parameters in terms of elastic, piezoelectric, dielectric, thermal and pyroelectric coefficients. The possibilities offered by those piezocomposite compositions are very sensitive to the considered piezoelectric phases and their volume fraction. As a result, these simulations are aimed at studying effect of the volume fraction of a constituent (piezoelectric ceramic phase) on the homogenized piezocomposite coefficients in order to predict its behavior while in service. It should also be noted that this model is based on the method applied to 1-3 piezocomposite in the context of characterizing thermoelectromechanical behavior. Hence it was difficult to find experimental data in the literature to compare the prediction results. However, with regard to the results provided by this model, we find some similarity of the curves with those of the 1-3 piezocomposite. This allows us to give some credibility to the developed model and therefore to validate it. As a perspective, it will be interesting to carry out an experiment to validate experimentally this model, although it is acceptable with the data from the 1-3 piezocomposite.

References

[1] R. Turner, P. Fuierer, R. Newnham, T. Shrout, Materials for high temperature acoustic and vibration sensors: A review, Applied Acoustics 41 (4) (1994) 299–324. doi:10.1016/0003-682x(94)90091-4.

[2] G. W. Hunter, J. D. Wrbanek, R. S. Okojie, P. G. Neudeck, G. C. Fralick, L. Chen, J. Xu, G. M. Beheim, Development and application of high-temperature sensors and electronics for propulsion applications, in: V. Korman (Ed.), Sensors for Propulsion Measurement Applications, Vol. 6222, International Society for Optics and Photonics, SPIE, 2006, p. 622209. doi:10.1117/12.668458.

[3] S. Zhang, Y. Fei, B. H. T. Chai, E. Frantz, D. W. Snyder, X. Jiang, T. R. Shrout, Characterization of piezoelectric single crystal YCa4o(BO3)3 for high temperature applications, Applied Physics Letters 92 (20) (2008) 202905. doi:10.1063/1.2936276.

[4] E. Rosenkrantz, J. Y. Ferrandis, F. Augereau, T. Lambert, D. Fourmentel, X. Tiratay, An innovative acoustic sensor for in-pile fission gas composition measurements, IEEE Transactions on Nuclear Science 60 (2) (2013) 1346–1353. doi:10.1109/tns.2013.2252624.

[5] E. Akdogan, M. Allahverdi, A. Safari, Piezoelectric composites for sensor and actuator applications, IEEE Transactions on Ultrasonics, Ferroelectrics and Frequency Control 52 (5) (2005) 746–775. doi:10.1109/tuffc.2005.1503962.

[6] H. Lee, S. Zhang, Y. Bar-Cohen, S. Sherrit, High temperature, high power piezoelectric composite transducers, Sensors 14 (8) (2014) 14526–14552. doi:10.3390/s140814526.

[7] R. Kar-Gupta, T. A. Venkatesh, Electromechanical response of 2-2 layered piezoelectric composites, Smart Materials and Structures 22 (2) (2013) 025035. doi:10.1088/0964-1726/22/2/025035.
URL https://doi.org/10.1088/0964-1726/22/2/025035

[8] W. Smith, Limits to the enhancement of piezoelectric transducers achievable by materials engineering, in: IEEE 1992 Ultrasonics Symposium Proceedings, 1992, pp. 697–702 vol.1. doi:10.1109/ULTSYM.1992.275912.

[9] W. A. Smith, New opportunities in ultrasonic transducers emerging from innovations in piezoelectric materials, New Developments in Ultrasonic Transducers and Transducer Systems 1733 (9) (1992) 3–26. doi:10.1117/12.130585.
URL https://www.spiedigitallibrary.org/conference-proceedings-of-spie/1733/0000/New-opportunities-in-ultrasonic-transducers-emerging-from-innovations-in-piezoelectric/.full

[10] T. R. Shrout, Innovations in piezoelectric materials for ultrasound transducers, 2008 17th IEEE International Symposium on the Applications of Ferroelectrics 3 (9) (2008) 1–4. doi:10.1109/ISAF.2008.4693822.
URL https://www.spiedigitallibrary.org/conference-proceedings-of-spie/3341/0000/Innovations-in-piezoelectric-materials-for-ultrasound-transducers/.full

[11] W. Qi, W. Cao, Finite element analysis and experimental studies on the thickness resonance of piezocomposite transducers, Ultrasonic Imaging 18 (1) (1996) 1–9. doi:10.1006/uimg.1996.0001.
URL https://www.sciencedirect.com/science/article/pii/S0161734696900012

[12] Q. Zhang, J. Chen, H. Wang, J. Zhao, L. Cross, M. Trottier, A new transverse piezoelectric mode 2-2 piezocomposite for underwater transducer applications, IEEE Transactions on Ultrasonics, Ferroelectrics, and Frequency Control 42 (4) (1995) 774–781. doi:10.1109/58.393119.

[13] J. Xu, Z. Han, N. Wang, Z. Li, J. Lv, X. Zhu, Y. Cui, X. Jian, Micromachined high frequency 1-3 piezocomposite transducer using picosecond laser, IEEE Transactions on Ultrasonics, Ferroelectrics, and Frequency Control 68 (6) (2021) 2219–2226. doi:10.1109/TUFFC.2021.3059942.

[14] A. Balé, R. Rouffaud, F. Levassort, R. Brenner, A.-C. Hladky-Hennion, Homogenization of periodic 1-3 piezocomposite using wave propagation: Toward an experimental method, The Journal of the Acoustical Society of America 149 (5) (2021) 3122–3132, publisher: Acoustical Society of America. doi:10.1121/10.0004824.
URL https://asa.scitation.org/doi/abs/10.1121/10.0004824

[15] D. Chen, C. Hou, C. Fei, D. Li, P. Lin, J. Chen, Y. Yang, An optimization design strategy of 1-3 piezocomposite ultrasonic transducer for imaging applications, Materials Today Communications 24 (2020) 100991. doi:10.1016/j.mtcomm.2020.100991.
URL https://www.sciencedirect.com/science/article/pii/S2352492820302130

[16] J. A. Krishnaswamy, F. C. Buroni, R. Melnik, L. Rodriguez-Tembleque, A. Saez, Design of polymeric auxetic matrices for improved mechanical coupling in lead-free piezocomposites, Smart Materials and Structures 29 (5) (2020) 054002, publisher: IOP Publishing. doi:10.1088/1361-665X/ab7e35.
URL https://doi.org/10.1088/1361-665x/ab7e35

[17] C. Peng, M. Chen, H. K. Sim, Y. Zhu, X. Jiang, Noninvasive and nonocclusive blood pressure monitoring via a flexible piezocomposite ultrasonic sensor, IEEE Sensors Journal 21 (3) (2021) 2642–2650. doi:10.1109/JSEN.2020.3021923.

[18] A. Agbossou, H. N. Viet, J. Pastor, Homogenization techniques and application to piezoelectric composite materials, International Journal of Applied Electromagnetics and Mechanics 10 (5) (1999) 391–403. doi:10.3233/jae-1999-154.

[19] H. Bisheh, T. Rabczuk, N. Wu, Effects of nanotube agglomeration on wave dynamics of carbon nanotube-reinforced piezocomposite cylindrical shells, Composites Part B: Engineering 187 (2020) 107739. doi:10.1016/j.compositesb.2019.107739.
URL https://www.sciencedirect.com/science/article/pii/S1359836819359529

[20] X. Gao, M. Zheng, X. Yan, J. Fu, Y. Hou, M. Zhu, High performance piezocomposites for flexible device application, Nanoscale 12 (8) (2020) 5175–5185. doi:10.1039/D0NR00111B.
URL https://pubs.rsc.org/en/content/articlelanding/2020/nr/d0nr00111b

[21] R. de Medeiros, R. Rodríguez-Ramos, R. Guinovart-Díaz, J. Bravo-Castillero, J. A. Otero, V. Tita, Numerical and analytical analyses for active fiber composite piezoelectric composite materials, Journal of Intelligent Material Systems and Structures 26 (1) (2015) 101–118. doi:10.1177/1045389x14521881.

[22] Q. Chen, W. Tu, R. Liu, X. Chen, Parametric multiphysics finite-volume theory for periodic composites with thermo-electro-elastic phases, Journal of Intelligent Material Systems and Structures 29 (4) (2017) 530–552. doi:10.1177/1045389x17711789.

[23] R. Newnham, D. Skinner, L. Cross, Connectivity and piezoelectric-pyroelectric composites, Mater. Res. Bull 5 (13) (1978) 525–536.

[24] H. Banno, Recent developments of piezoelectric ceramic products and composites of synthetic rubber and piezoelectric ceramic particles, Ferroelectrics 50 (1) (Nov. 1983). doi:10.1080/00150198308014425.
URL https://doi.org/10.1080/00150198308014425

[25] T. Furukawa, K. Fujino, E. Fukada, Electromechanical properties in the composites of epoxy resin and PZT ceramics, Japanese Journal of Applied Physics 15 (11) (1976) 2119. doi:10.1143/JJAP.15.2119.
URL https://iopscience.iop.org/article/10.1143/JJAP.15.2119/meta

[26] R. Steinhausen, T. Hauke, W. Seifert, H. Beige, W. Watzka, S. Seifert, D. Sporn, S. Starke, A. Schönecker, Finescaled piezoelectric 1-3 composites: properties and modeling, Journal of the European Ceramic Society 19 (6) (1999) 1289–1293. doi:10.1016/S0955-2219(98)00422-1.
URL https://www.sciencedirect.com/science/article/pii/S0955221998004221

[27] H. L. W. Chan, P. K. L. Ng, C. L. Choy, Effect of poling procedure on the properties of lead zirconate titanate/vinylidene fluoride-trifluoroethylene composites, Applied Physics Letters 74 (20) (1999) 3029–3031. doi:10.1063/1.124054.

URL https://aip.scitation.org/doi/abs/10.1063/1.124054

[28] K. L. Ng, H. L. W. Chan, C. L. Choy, Piezoelectric and pyroelectric properties of PZT/PVDF-TrFE composites with constituent phases poled in parallel or antiparallel directions, IEEE Transactions on Ultrasonics, Ferroelectrics, and Frequency Control 47 (6) (2000) 1308–1315. doi:10.1109/58.883519.

[29] M. L. Dunn, M. Taya, Micromechanics predictions of the effective electroelastic moduli of piezoelectric composites, International Journal of Solids and Structures 30 (2) (1993) 161–175. doi:10.1016/0020-7683(93)90058-F.
URL https://www.sciencedirect.com/science/article/pii/002076839390058F

[30] N. Mishra, K. Das, A comparative study of incremental selfconsistent and eshelby-mori-tanaka models for estimating the electroelastic properties of piezoelectric polymer composites with an orthotropic matrix, Mechanics of Composite Materials 58 (5) (2022) 657–672. doi:10.1007/s11029-022-10057-8.

[31] W.-S. Kuo, J. H. Huang, On the effective electroelastic properties of piezoelectric composites containing spatially oriented inclusions, International Journal of Solids and Structures 34 (19) (1997) 2445–2461. doi:10.1016/S0020-7683(96)00154-0.
URL https://www.sciencedirect.com/science/article/pii/S0020768396001540

[32] C.-W. Nan, L. Liu, D. Guo, L. Li, Calculations of the effective properties of 1-3 type piezoelectric composites with various rod/fibre orientations, Journal of Physics D: Applied Physics 33 (22) (2000) 2977–2984. doi:10.1088/0022-3727/33/22/317.
URL https://doi.org/10.1088/0022-3727/33/22/317

[33] G. M. Odegard, Constitutive modeling of piezoelectric polymer composites, Acta Materialia 52 (18) (2004) 5315–5330. doi:10.1016/j.actamat.2004.07.037.
URL https://www.sciencedirect.com/science/article/pii/S135964540400446X

[34] N. Fakri, L. Azrar, Thermal and electroelastic behavior of piezocomposites and inhomogeneous piezoelectric materials with voids, Journal of Intelligent Material Systems and Structures 21 (2) (2009) 161–174. doi:10.1177/1045389x09352815.

[35] R. Kar-Gupta, T. A. Venkatesh, Electromechanical response of 1-3 piezoelectric composites: An analytical model, Acta Materialia 55 (3) (2007) 1093–1108. doi:10.1016/j.actamat.2006.09.023.
URL https://www.sciencedirect.com/science/article/pii/S1359645406007038

[36] K. Hashimoto, M. Yarnaguchi, Elastic, piezoelectric and dielectric properties of composite materials, in: IEEE 1986 Ultrasonics Symposium, 1986, pp. 697–702. doi:10.1109/ULTSYM.1986.198824.

[37] H. Taunaumang, I. L. Guy, H. L. W. Chan, Electromechanical properties of 1-3 piezoelectric ceramic/piezoelectric polymer composites, Journal of Applied Physics 76 (1) (1994) 484–489. doi:10.1063/1.357099.
URL https://aip.scitation.org/doi/abs/10.1063/1.357099

[38] C. N. Della, D. Shu, The performance of 1-3 piezoelectric composites with a porous non-piezoelectric matrix, Acta Materialia 56 (4) (2008) 754–761. doi:10.1016/j.actamat.2007.10.022.
URL https://www.sciencedirect.com/science/article/pii/S1359645407007136

[39] F. Levassort, M. Pham-Thi, H. Hemery, P. Maréchal, L. Tran-Huu-Hue, M. Lethiecq, Piezoelectric textured ceramics: effective properties and application to ultrasonic transducers, Ultrasonics 44 (2006) 621–626. doi:10.1016/j.ultras.2006.05.016.
URL https://www.sciencedirect.com/science/article/pii/S0041624X06000448

[40] F. Levassort, M. Pham-Thi, P. Maréchal, L. Tran-Huu-Hue, M. Lethiecq, Ultrasonic transducer based on highly textured PMN-PT piezoelectric ceramic, Journal of Electroceramics 19 (4) (2007) 375–381. doi:10.1007/s10832-007-9176-5.
URL https://link.springer.com/article/10.1007/s10832-007-9176-5

[41] P. Tize Mha, P. Maréchal, G. E. Ntamack, S. Charif d'Ouazzane, Homogenized electromechanical coefficients and effective parameters of 1-3 piezocomposites for ultrasound imaging transducers, Physics Letters A 408 (2021) 127492. doi:10.1016/j.physleta.2021.127492.
URL https://www.sciencedirect.com/science/article/pii/S037596012100356X

[42] Q. Zhang, W. Cao, J. Zhao, L. Cross, Piezoelectric performance of piezoceramic-polymer composites with 2-2 connectivity - A combined theoretical and experimental study, IEEE Transactions on Ultrasonics, Ferroelectrics, and Frequency Control 41 (4) (1994) 556–564. doi:10.1109/58.294118.

[43] K. S. Challagulla, T. A. Venkatesh, Electromechanical response of 2-2 layered piezoelectric composites: A micromechanical model based on the asymptotic homogenization method, Philosophical Magazine 89 (14) (2009) 1197–1222. doi:10.1080/14786430902915412.
URL https://www.tandfonline.com/doi/abs/10.1080/14786430902915412

[44] M. Sakthivel, A. Arockiarajan, An analytical model for predicting thermo-electro-mechanical response of 1-3 piezoelectric composites, Computational Materials Science 48 (4) (2010) 759–767. doi:10.1016/j.commatsci.2010.03.027.
URL https://www.sciencedirect.com/science/article/pii/S0927025610001497

[45] S. Iyer, T. A. Venkatesh, Electromechanical response of (3-0,3-1) particulate, fibrous, and porous piezoelectric composites with anisotropic constituents: A model based on the homogenization method, International Journal of Solids and Structures 51 (6) (2014) 1221–1234. doi:10.1016/j.ijsolstr.2013.12.008.
URL https://www.sciencedirect.com/science/article/pii/S0020768313004812
[46] F. L. Hanse Wampo, R. P. Lemanle Sanga, P. Maréchal, G. E. Ntamack, Piezocomposite transducer design and performance for high resolution ultrasound imaging transducers, International Journal of Computational Materials Science and Engineering 08 (03) (2019) 1950013. doi:10.1142/s2047684119500131.
[47] F. L. H. Wampo, R. Ntenga, J. Y. Effa, Y. Lapusta, G. E. Ntamack, P. Maréchal, Generalized homogenization model of piezoelectric materials for ultrasonic transducer applications, Journal of Composite Materials 56 (5) (2021) 713–726. doi:10.1177/00219983211058806.
[48] N. Pakam, A. Arockiarajan, Study on effective properties of 1-3-2 type magneto-electro-elastic composites, Sensors and Actuators A: Physical 209 (2014) 87–99. doi:10.1016/j.sna.2014.01.009.
URL https://www.sciencedirect.com/science/article/pii/S0924424714000119
[49] M. Sakthivel, A. Arockiarajan, An effective matrix poling characteristics of 1-3-2 piezoelectric composites, Sensors and Actuators A: Physical 167 (1) (2011) 34–43. doi:10.1016/j.sna.2011.01.004.
URL https://www.sciencedirect.com/science/article/pii/S0924424711000082
[50] M. Sakthivel, A. Arockiarajan, Thermo-electro-mechanical response of 1-3-2 type piezoelectric composites, Smart Materials and Structures 19 (10) (2010) 105033. doi:10.1088/0964-1726/19/10/105033.
URL https://doi.org/10.1088/0964-1726/19/10/105033
[51] S. Yi, W. Zhang, G. Gao, H. Xu, D. Xu, Structural design and properties of fine scale 2-2-2 PZT/epoxy piezoelectric composites for high frequency application, Ceramics International 44 (9) (2018) 10940–10944. doi:10.1016/j.ceramint.2018.03.165.
URL https://www.sciencedirect.com/science/article/pii/S0272884218307314
[52] V. Levin, M. Rakovskaja, W. Kreher, The effective thermoelectroelastic properties of microinhomogeneous materials, International Journal of Solids and Structures 36 (18) (1999) 2683–2705. doi:10.1016/s0020-7683(98)00131-0.
[53] V. Levin, M. Rakovskaja, W. Kreher, Erratum to "the effective thermoelectroelastic properties of microinhomogeneous materials" [international journal of solids and structures 36 (1999) 2683-2705], International Journal of Solids and Structures 37 (52) (2000) 7821. doi:10.1016/s0020-7683(99)00336-4.
[54] J. H. C. Cha, J. H. Chang, Development of 15 MHz 2-2 piezo-composite ultrasound linear array transducers for ophthalmic imaging, Sensors and Actuators A: Physical 217 (9) (2014) 39–48. doi:10.1016/j.sna.2014.06.024.
URL https://www.sciencedirect.com/science/article/pii/S0924424714003197
[55] A. Reuss, Berechnung der fließgrenze von mischkristallen auf grund der plastizitätsbedingung für einkristalle ., ZAMM - Zeitschrift für Angewandte Mathematik und Mechanik 9 (1) (1929) 49–58. doi:10.1002/zamm.19290090104.

Appendix A.

$$
\begin{aligned}
\overline{d}_{31} &= \nu_f \left(A_4 s^f_{12} + B_4 s^f_{13} + d^f_{31} - A_4 s^m_{12} - B_4 s^m_{13} \right) + \nu_m d^m_{31} \\
\overline{d}_{32} &= d^f_{32} + A_4 s^f_{22} + B_4 s^f_{23} \\
\overline{d}_{33} &= d^f_{33} + A_4 s^f_{23} + B_4 s^f_{33} \\
\overline{s}_{11} &= \nu_f \left(A_1 s^f_{12} + B_1 s^f_{13} + s^f_{11} - A_1 s^m_{12} - B_1 s^m_{13} \right) + \nu_m s^m_{11} \\
\overline{s}_{12} &= \nu_f \left(A_2 s^f_{12} + B_2 s^f_{13} - A_2 s^m_{12} - B_2 s^m_{13} \right) + s^m_{12} \\
\overline{s}_{13} &= \nu_f \left(A_3 s^f_{12} + B_3 s^f_{13} - A_3 s^m_{12} - B_3 s^m_{13} \right) + s^m_{13} \\
\overline{s}_{23} &= A_3 s^f_{22} + B_3 s^f_{23} \\
\overline{s}_{22} &= A_2 s^f_{22} + B_2 s^f_{23} \\
\overline{s}_{33} &= A_3 s^f_{23} + B_3 s^f_{33} \\
\overline{\varepsilon}^T_{33} &= \nu_f \left(A_4 d^f_{32} + B_4 d^f_{33} + \varepsilon^{T,f}_{33} - A_4 d^m_{32} - B_4 d^m_{33} \right) + \nu_m \varepsilon^{T,m}_{33}
\end{aligned}
$$

Appendix B.

$$
\begin{aligned}
A_1 &= \nu_m \left(s_{12}^m - s_{12}^f\right) K_1 - \nu_m \left(s_{13}^m - s_{13}^f\right) K_2 \\
A_2 &= s_{22}^m K_1 - s_{23}^m K_2 \\
A_3 &= s_{23}^m K_1 - s_{33}^m K_2 \\
A_4 &= \nu_m \left(d_{32}^m - d_{32}^f\right) K_1 - \nu_m \left(d_{33}^m - d_{33}^f\right) K_2 \\
B_1 &= \nu_m \left(s_{13}^m - s_{13}^f\right) K_3 - \nu_m \left(s_{12}^m - s_{13}^f\right) K_2 \\
B_2 &= s_{23}^m K_3 - s_{22}^m K_2 \\
B_3 &= s_{33}^m K_3 - s_{23}^m K_2 \\
B_4 &= \nu_m \left(d_{33}^m - d_{33}^f\right) K_3 - \nu_m \left(d_{32}^m - d_{32}^f\right) K_2
\end{aligned}
$$

Appendix C.

$$
\begin{aligned}
K_1 &= \frac{\left(\nu_m s_{33}^f + \nu_f s_{33}^m\right)}{\left(\nu_m s_{22}^f + \nu_f s_{22}^m\right)\left(\nu_m s_{33}^f + \nu_f s_{33}^m\right) - \left(\nu_m s_{23}^f + \nu_f s_{23}^m\right)^2} \\
K_2 &= \frac{\left(\nu_m s_{23}^f + \nu_f s_{23}^m\right)}{\left(\nu_m s_{22}^f + \nu_f s_{22}^m\right)\left(\nu_m s_{33}^f + \nu_f s_{33}^m\right) - \left(\nu_m s_{23}^f + \nu_f s_{23}^m\right)^2} \\
K_3 &= \frac{\left(\nu_m s_{22}^f + \nu_f s_{22}^m\right)}{\left(\nu_m s_{22}^f + \nu_f s_{22}^m\right)\left(\nu_m s_{33}^f + \nu_f s_{33}^m\right) - \left(\nu_m s_{23}^f + \nu_f s_{23}^m\right)^2}
\end{aligned}
$$